RESEARCH PAPER | Engineering | Volume : 3 | Issue : 11 | Nov 2013 | ISSN - 2249-555X

Integration of Hybrid Multilevel Inverter using Space Vector Modulation Technique

KEYWORDS: DC/AC power conversion, multilevel inverter, DER, MPPT, Integration of Renewable Energy Sources, Wind Power, Solar, Battery Energy

A.Ramesh	M.Siva Kumar	M.UmaVani
Associate Professor Aditya Engineering College, Surampalem, A.P, India	Professor, Gudlavalleru Engineering College, Gudlavalleru, AP, India	Professor, K. L. University,Vijayawada, AP, India

ABSTRACT *This paper proposes a new power-control strategy for grid-connected generation systems with versatile power transfer. Wind, Solar, Fuel cell and Battery systems are integrated in this work. An adaptive Maximum power point tracking system (MPPT) algorithm along with standard perturbs and observes method has been implemented. This system allows maximum utilization of freely available renewable energy sources like wind, fuel and photovoltaic energies.*

The objective of this work is to implement a novel five and seven level multi-string inverter topology for Distributed Energy resources (DER) based DC/AC conversion system. A high step-up converter is introduced as a front-end stage to improve the conversion efficiency of conventional boost converters and to stabilize the output DC voltage of various DERs. The proposed multilevel inverter requires only six active switches instead of eight as required in the conventional cascaded H-Bridge (CCHB) inverter.

The DC output from non-conventional energy source is converted into AC power for synchronizing with the grid. This hybrid system operates under normal and abnormal conditions with the support of the Battery Supply. The simulation results are presented to illustrate the operating principle, feasibility, and reliability of this proposed system.

I. INTRODUCTION

Nowadays, photovoltaic (PV) energy appears quite attractive for electricity generation because of its noiseless, pollution-free, scale flexibility, and little maintenance. The PV power generation depends on sun irradiation level, ambient temperature, and unpredictable shadows [1]. A PV-based power system should be supplemented by other alternative energy sources to ensure a reliable power supply. Fuel cells (FCs) are emerging as a promising supplementary power sources due to their merits of cleanliness, high efficiency, and high reliability. Because of long startup period and slow dynamic response weak points of FCs [2], mismatch power between the load and the FC must be managed by an energy storage system. Batteries are usually taken as storage mechanisms for smoothing output power, improving startup transitions and dynamic characteristics, and enhancing the peak power capacity [3,4]. Combining such energy sources introduces a PV/Wind/FC/battery hybrid power system. In comparison with single-sourced systems, the hybrid power systems have the potential to provide high quality, more reliable, and efficient power.

In these systems with a storage element, the bidirectional power flow capability is a key feature at the storage port. Further input power sources should have the ability of supplying the load individually and simultaneously. Many hybrid power systems with various power electronic converters have been proposed in the literature up to now. Traditional methods that integrate different power sources to form a hybrid power system can be classified into AC coupled systems [5,6].

However, the main shortcomings of these traditional integrating methods are complex system topology, high count of devices, high power losses, expensive cost, and large size. In recent years, several power conversion stages used in traditional hybrid systems are replaced by multi-input converters (MICs), which combine different power sources in a single power structure. These converters have received more attention in the literature because of providing simple circuit topology, centralized control, bidirectional power flow for the storage element, high reliability, and low manufacturing cost and size. In general, the systematic approach of generating MICs is introduced in [7], in which the concept of the pulsating voltage source cells and the pulsating current source cells is proposed for deriving MICs. One of the samples of these MICs is utilized in [8] to hybridize PV and wind power sources in a unified structure.

A systematic method to synthesize MICs is proposed in [9]. Assumptions, restrictions, and conditions used in analyzing MICs are described in [10], and it lists some basic rules that allow feasible and un- feasible input cells that realize MICs from their single-input versions. Two multiple-input converters based on flux additivity in a multi winding transformer are reported in [11]. Because there was no possibility of bidirectional operating of the converter in [11], and complexity of driving circuits and output power limitation [12], they are not suitable for hybrid systems. In [13], a three port bidirectional converter with three active full bridges, two series resonant tanks, and a three- winding high-frequency transformer are proposed. In comparison with three-port circuits with only inductors and Diode Bridge at the load side, it gives higher boost gain and reduced switching losses due to soft-switching operation.

In this work, a power control strategy is designed to manage the charge balance of the battery in order to regulate the output voltage. In these systems, the PV and the wind sources are exploited in MPPT conditions. Moreover, control strategies of the both systems are designed based on small signal modeling of the converters.

A new four input DC-DC boost converter is proposed for hybrid power system applications. The proposed converter interfaces three unidirectional ports for input power sources, a bidirectional port for a storage element, and a port for output load in a unified structure. The converter is current source type at all three input power ports and is able to step up the input voltages. The proposed structure utilizes only four power switches that are independently controlled with four different duty ratios. These duty ratios facilitate controlling of power flow from the input sources. Power from the input power sources can be delivered to the load individually or

Volume : 3 | Issue : 11 | Nov 2013 | ISSN - 2249-555X

simultaneously.

A novel five and seven level multistring inverter topology for DERs based DC/AC conversion system is implemented in this work. A high step-up converter is introduced as a front end stage to improve the conversion efficiency of conventional boost converters and to stabilize the output DC voltage of various DERs such as PV, Wind and fuel cell modules for use with the simplified newly constructed multilevel inverter. The proposed multilevel inverter requires only six active switches instead of the eight required in the conventional cascaded H- bridge (CCHB) multilevel inverter. Switches are controlled with SVM technique.

II. POWER CONTROL TECHNIQUES FOR CONVERTER STAGES

A. High Power Converter Stage

In this study, high Power converter topology is introduced to boost and stabilize the output DC voltage of various DERs such as PV, Wind and Fuel cell modules for employment of the proposed simplified multilevel inverter.

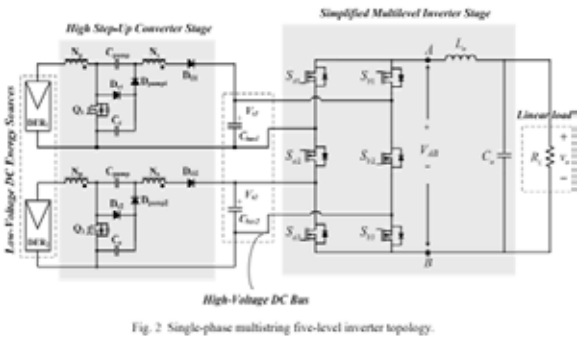

Fig. 2 Single-phase multistring five-level inverter topology.

Fig. 1 Single Phase Multi String Inverter Topology

The coupled inductor of the boost converter shown in Fig. 1 can be modeled as an ideal transformer, a magnetizing inductor, and a leakage inductor. According to the voltage balance condition of the magnetizing inductor the voltage of the primary winding can be derived as

$$V_{pri} = V_{in} \cdot \frac{D}{(1-D)} \quad (1)$$

Where V_{in} represents each the low-voltage DC energy input sources, and voltage of the secondary winding is given by

$$V_{sec} = \frac{N_S}{N_P} \cdot V_{Pri} = \frac{N_S}{N_P} \cdot V_{in} \cdot \frac{D}{(1-D)} \quad (2)$$

Similar to that of the boost converter, the voltage of the charge-pump capacitor C_{pump} and clamp capacitor Cc can be expressed as

$$V_{cp} = V_{Cc} = V_{in} \cdot \frac{D}{(1-D)} \quad (3)$$

Hence, the voltage conversion ratio of the high step-up converter, named input voltage to bus voltage ratio, can be derived as [14]

$$\frac{V_{si}}{V_{in}} = \left(2 + \frac{N_s}{N_p} \cdot \frac{D}{(1-D)}\right)\Big|_{i=1,2} \quad (4)$$

B. Simplified Multilevel Inverter Stage

It should be assumed that, in this configuration the three capacitors in the capacitive voltage divider are connected directly across the DC bus as shown in Fig. 2, and all switching combinations are activated in an output cycle. The capacitors are configured to maintain a constant voltage at the common DC Bus. Wind Generator along with rectifier is shown in a single block. The dynamic voltage balance between the three capacitors is automatically controlled by the preceding high step-up converter stage. Then, we can assume $V_{s1}=V_{s2}=V_{s3}=Vs$.

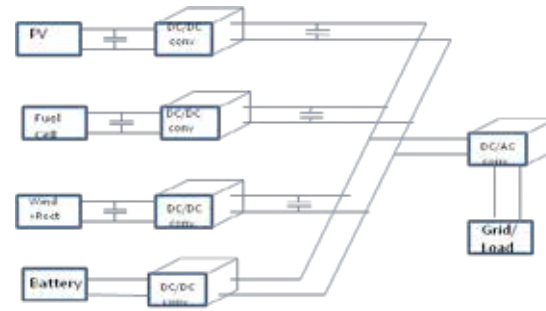

Fig.2. Configuration of Multi String Inverter Topology

A new single-phase multi string topology is used whose basic circuit is presented in Fig.3 to solve problems associated with multiple power stages and complex control circuits. This topology includes six power switches which are less than those of CCHB inverter with eight power switches. This reduces the complexity in power circuit and simplifies modulator circuit design and implementation. The Phase disposition Pulse Width Modulation (PDPWM) control scheme is introduced to generate switching signals and to produce five output-voltage levels: zero, V_S, $2V_S$, $-V_S$, and $-2V_S$.

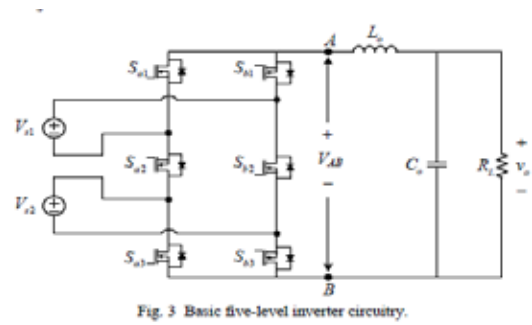

Fig. 3 Basic five-level inverter circuitry.

Fig.3. Basic five-level inverter circuitry.

This inverter topology uses two carrier signals and one reference to generate PWM signals for the switches. The modulation strategy and its logic scheme implemented are shown in Fig.4. This is a widely used alternative technique for phase disposition modulation. With the exception of an offset value equivalent to the carrier signal amplitude, two comparators are used in this scheme with identical carrier signals V_{tri1} and V_{tri2} to provide high-frequency switching signals for switches S_{a1}, S_{b1}, S_{a3} and S_{b3}. Another comparator is used for zero crossing detection to provide line-frequency switching signals for switches S_{a2} and S_{b2}.

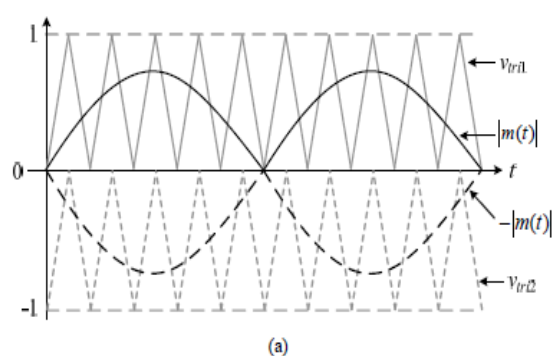

Fig. 4. Switching Scheme

Volume : 3 | Issue : 11 | Nov 2013 | ISSN - 2249-555X

For convenient illustration, the switching function of the switch in Fig. 3 is defined as follows

$$S_{aj} = \begin{cases} 1, & S_{aj} \text{ ON} \\ 0, & S_{aj} \text{ OFF} \end{cases}, j=1, 2, 3 \quad (5)$$

$$S_{bj} = \begin{cases} 1, & S_{bj} \text{ ON} \\ 0, & S_{bj} \text{ OFF} \end{cases}, j = 1,2,3 \quad (6)$$

Table I. lists switching combinations that generate the required five output levels. The corresponding operation modes of the multilevel inverter stage are described clearly as follows

Table-I Switching Combinations

S_{a1}	S_{a2}	S_{a3}	S_{b1}	S_{b2}	S_{b3}	V_{AB}
0	1	0	1	0	1	$2V_s$
0	1	1	1	0	0	V_s
1	1	0	0	0	1	V_s
1	1	1	0	0	0	0
0	0	0	1	1	1	0
1	0	0	0	1	1	$-V_s$
0	0	1	1	1	0	$-V_s$
1	0	1	0	1	0	$-2V_s$

The control signal block is shown in Fig.4 m(t) is the sinusoidal modulation signal. Both V_{tri1} and V_{tri2} are the two triangular carrier signals. The peak value and frequency of the sinusoidal modulation signal are given as m_{peak}=0.7 and f_m=60Hz, respectively. The peak-to-peak value of the triangular modulation signal is equal to 1, and the switching frequency f_{tri1} and f_{tri2} are both considered as 1.8 kHz.

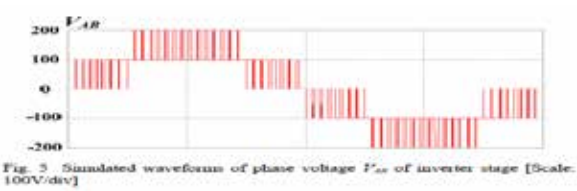

Fig. 5 Simulated waveforms of phase voltage V_{AB} of inverter stage [Scale: 100V/div]

Fig. 5 Simulated waveforms for phase voltage V_{AB} of inverter stage [Scale: 100V/div]

The three input voltage sources feeding from the high step-up converter is controlled at 100V on DC Bus, i.e. V_{S1}=V_{S2}=V_{S3}=V_S=100V. The simulated waveform of the phase voltage with five levels is shown in Fig. 5. The switch voltages of S_{a1}, S_{a2}, S_{a3}, S_{b1}, S_{b2}, and S_{b3} are all shown in Fig. 6. It is evident that the voltage stresses of the switches S_{a1}, S_{a3}, S_{b1}, and S_{b3} are all equal to 100V, and only the other two switches S_{a2}, S_{b2} must be 200V voltage stress.

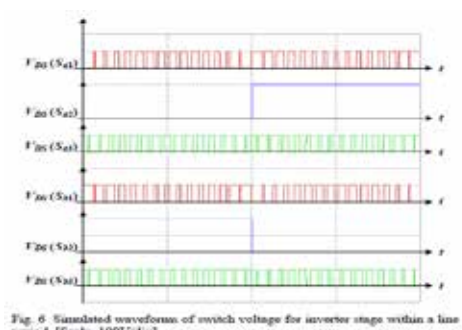
Fig. 6 Simulated waveforms of switch voltage for inverter stage within a line period. [Scale: 100V/div]

Fig.6 simulated waveforms of switch voltage for inverter stage with in a line period

[Scale: 100V/div]

$$P_s = 0.5V_{DS}I_0f_s[t_{c(on)} + t_{c(off)}] \quad (7)$$

V_{DS} is the voltage across each switch; and I_o is the entire current which flows through the switch.

Compared with the CCHB circuit topology as shown in Fig.7, the voltage stresses of the eight switches of the CCHB inverter are all equal to V_s. For simplification, both the proposed circuit and CCHB inverter are operated at the same turn-on and turn-off crossover intervals and at the same load I_o. Then, the average switching power loss P_s is proportional to V_{DS} and f_s as

$$P_s \alpha V_{DS}.f_s \quad (8)$$

According to Eq. (8) and Table I the switching losses of the CCHB inverter from eight switches can be, obtained as

$$P_{s,\ H\text{-}bridge} \alpha 8V_sf_s \quad (9)$$

Similarly, the switching power loss of the proposed single-phase five-level inverter due to six switches can also be obtained as

$$P_{s,\ proposed} \alpha 4V_s*f_s + 2(2V_s)\, f_m \alpha 4V_s\,(f_s+f_m). \quad (10)$$

Because switches S_{a2}, S_{b2} can only be activated twice in a line period (60Hz) and the switching frequency is larger than the line frequency (f_s>>f_m), the switching losses of the proposed circuit is approximated to $4V_s*f_s$. Obviously, the switching power loss is nearly half that of the CCHB inverter.

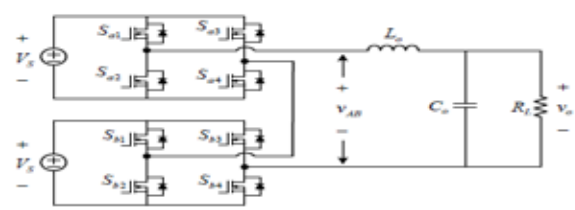
Fig. 7 Five-level inverter topologies of CCHB inverter [15].

Fig.7 Five-level inverter topologies of CCHB inverter

Considering the harmonics in the inverter output voltage V_{AB}, the amplitude of the fundamental and harmonic components in the output voltage V_{AB} are calculated by PSIM software. The phase shift PWM technique is adopted for the CCHB Inverter. Both of the CCHB multilevel inverter and the studied multilevel inverter are operated in the same condition, including the same switching frequency 18kHz, the same modulation index ma ,the same input voltage V_S=100V and output L-C filter, L_o= 420uH, C_o= 4.7uF.The studied multilevel inverter have lower THD than the CCHB multilevel inverter. It implies that the output waveform is improved and smaller filter size can be used.

C. DC-AC Power converter space vector modulation Technique.

6 power switches of inverter with 8 possible combinations shown in Figure. 3 are corresponding to effective voltage space vector U_1 - U_6 and 2 zero vectors U_0, U_7. The phase angle between one effective voltage space vector and adjacent one is 60 degrees. They constitute 6 uniform segments. The three digits in brackets express the linking state between three-phase output A,B,C and the input DC, such as M=101 which represents the switching of the switches S_{PA} ,S_{NB} and S_{PC}.The output voltage space vectors and the corresponding switching states are represented in "Fig. 8".

Volume : 3 | Issue : 11 | Nov 2013 | ISSN - 2249-555X

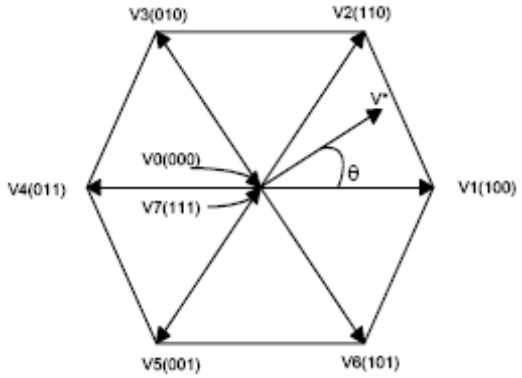

Fig. 8 the composition of output voltage vector and switching stages

Any expected output voltage space vector U_J is formed by adjacent two basic output voltage vectors U_M,U_N and zero output voltage U_o or U_7. Suppose the angle between U_J and U_M is θ_J

$$U_J=d_MU_M+d_NU_N+d_OU_O \quad (11)$$

Where d_M, d_N and d_0 are the ratio cycles of U_M, U_N and U_0 respectively. And

$$d_m=\frac{T_M}{T_g}=m_v\mathrm{Sin}(60-\theta_j) \quad (12)$$

$$d_m=\frac{T_M}{T_g}=m_v\mathrm{Sin}(\theta_j) \quad (13)$$

$$d_0=1-d_M-d_N \quad (14)$$

Where T_M, T_N is the switching time of vectors U_M and U_N respectively. T_g is the switching period of PWM.m_v is the modulation index of output voltage. And

$$m_{vm}\left(\frac{2}{3}\right)^{1/2}\frac{U_{0m}}{(U_{im}*m_c\ cos\emptyset)} \quad (15)$$

Where U_{0m} and U_{im} are the amplitudes of output and input voltages, m_c is the input current modulation index, generally set m_c =1. Ø is the input power factor angle. When the rotating space vector U_j locates in a segment, the local average of output voltage can be formed by two adjacent basic voltage space vectors constituting this segment and one zero voltage space vector.

D. S PWM Techniques

A different approach to SPWM is based on the space vector representation of voltages in the d, q plane. The d, q components are found by Park's transform, where the total power, as well as the impedance, remains unchanged.

Fig. 9 shows space vector modulation in accordance with 8 switching positions of inverter, V* is the phase-to-center voltage which is obtained by proper selection of adjacent vectors V1 and V2.

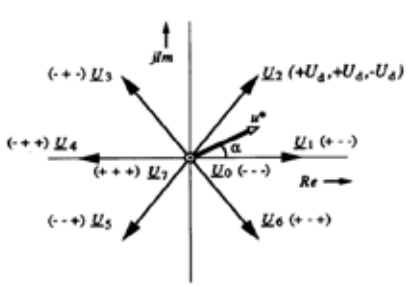

Fig. 9 Space Vector Modulation

The reference space vector V* is given by Equation (16), where T_1, T_2 are the intervals of application of vector V_1 and V_2 respectively, and zero vectors V_0 and V_7 are selected for T_0.

$$V^*\ Tz = V_1*T_1 + V_2*T_2 + V_0*(T_0/2) + V_7*(T_0/2) \quad (16)$$

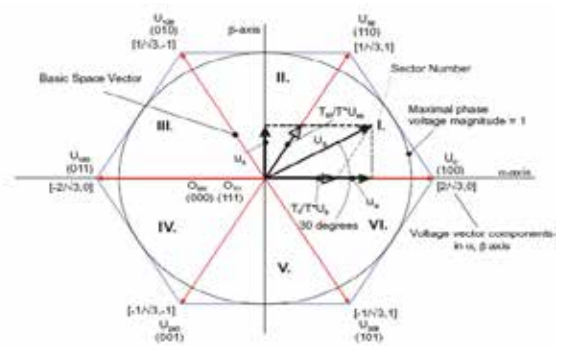

Fig. 10. Inverter output voltage space vector

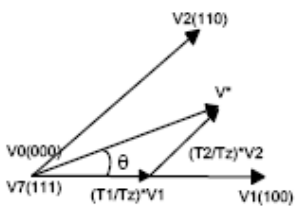

Fig. 11 Determination of Switching times

The amplitude of u0 and u7 equals to zero. The other vectors, u1, u2……u6 have the same amplitude and are shifted. By varying the relative switching on time of the different vectors, the space vector u* and also the output voltages U_a, U_b and U_c can be varied and is defined as

U_a= Real (U*),

U_b= Real (U*. a-1)

U_c= Real (U*. a-2) (17)

During a switching period, T_c, and considering the example of first vector, the vectors u0, u1 and u2 were switched on alternatively.

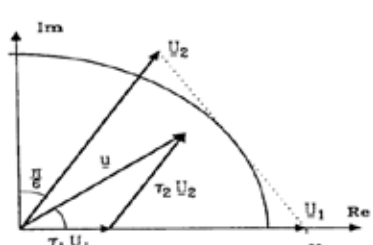

Fig. 12 Definition of the Space Vector

Depending on the switching times, t0, t1 and t2, the space vector u* can be defined as,

$U^* = 1/Tc.(t_0.u_0 + t_1.u_1 + t_2.u_2)$(18)

It can be simplified as,

$U^* = (t_0.u_0 + t_1.u_1 + t_2.u_2)$

This is equal to

Volume : 3 | Issue : 11 | Nov 2013 | ISSN - 2249-555X

$U^* = t_1.u_1 + t_2. u_2$

where,

$t_0 + t_1 + t_2 = T_c$ and

$t_0 + t_1 + t_2 = 1$

t_0, t_1 and t_2 are the relative values of the on switching times. They are defined as:

$t_1 = m * \cos(a + p/6)$

$t_2 = m * \sin a$ $t_0 = 1 - t_1 - t_2$

Their values are implemented in a table for a modulation factor m = 1. Then it will be easy to calculate the space vector U* and the output voltages U_a, U_b and U_c.The voltage vector U* can be provided directly by the optimal vector control laws w1, V_{Sa} and V_{Sb}. In order to generate the phase voltages U_a, U_b and U_c corresponding to the desired voltage vector U* the above SVM strategy is proposed.

III Simulation Results:

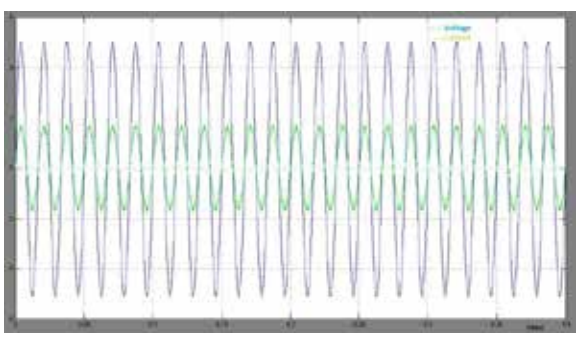

Fig13.Out put Voltage and Current with Unity Power factor

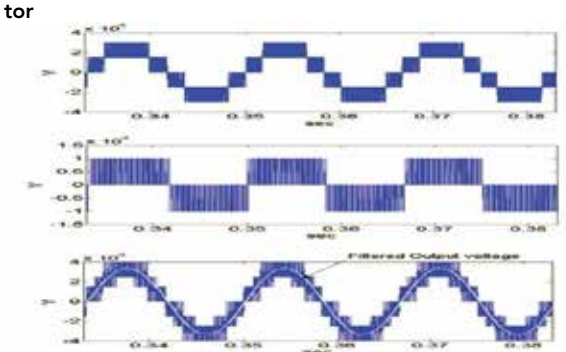

Fig14.Five Level Inverter out Put Voltage

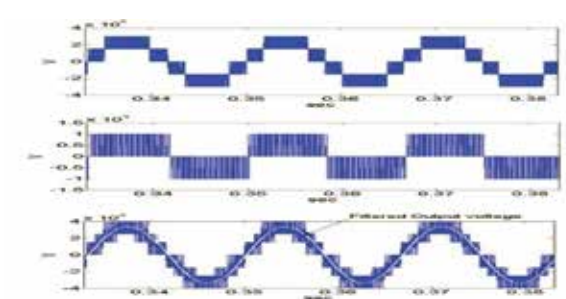

Fig15.Five line Voltage of Inverter

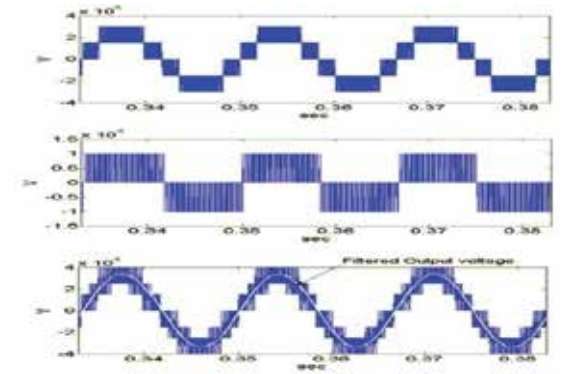

Fig16.Seven Level Voltage of Inverter

IV CONCLUSIONS:

This work reports a newly-constructed single & three -phase multi string Five and seven level inverter topology that produces a significant reduction in the number of power devices required to implement multilevel output for DERs. The proposed inverter topology offers strong advantages such as improved output waveforms, smaller filter size, and lower EMI and THD. Simulation results show the effectiveness of the proposed solution.

In this work, a high step-up converter is introduced as a front-end stage to improve the conversion efficiency of conventional boost converters and to stabilize the output DC voltage of various DERs such as PV, Wind and fuel cell modules for use with the simplified newly constructed multilevel inverter. The proposed multilevel inverter requires only six active switches instead of the eight required in the conventional cascaded H- bridge (CCHB) multilevel inverter, control with SVM technique.

The inverter converts the DC output from non-conventional energy into useful AC power for the connected load. This hybrid system operates under normal conditions which include conventional and proposed cases of solar energy, fuel and wind energy. The simulation results are presented to illustrate the operating principle, feasibility and reliability of this proposed system for Renewable resources.

Volume : 3 | Issue : 11 | Nov 2013 | ISSN - 2249-555X

REFERENCE

[1]Yi-Hun Liao, Ching-Ming Lai, "Newly-Constructed Simplified Single-Phase Multi-string Multilevel Inverter Topology for Distributed Energy Resources" IEEE Transactions on Power Electronics, Volume: 26, Issue: 9 . Sept, 2011 | [2]Y. Li, D. M. Vilathgamuwa, and P. C. Loh, "Design, analysis, and real-time testing of a controller for multi bus microgrid system" IEEE Trans. Power Electronics vol. 19, no. 5, pp. 1195-1204, Sept. 2004. | [3]N. Hatziargyriou, H. Asano, R. Iravani, and C. Marnay, "Micro grids, IEEE Power and Energy Magazine" vol. 5, no. 4, pp. 78-94, Jul./Aug. 2007. | [4 F. Katiraei, R. Iravani, N. Hatziargyriou, and A. Dimeas, "Micro-grids management" IEEE Power and Energy Magazine, vol. 6, no. 3, pp. 54- 65, May/Jun., 2008. | [5] C. L. Chen, Y. Wang, J.S.Lai, Y.S.Lee, and D. Martin, "Design of parallel inverters for smooth mode transfer micro-grid applications" IEEE Trans. Power Electronics vol. 25, no. 1, pp. 6-15, Jan. 2010. | [6] C. T. Pan, C. M. Lai, and M. C. Cheng, "A novel high step-up ratio inverter for distributed energy resources (DERs)" IEEE International Power Electronics Conference-ECCE Asia, pp.1433-1437, 2010. | [7] N. A. Rahim and J. Selvaraj, "Multi string five-level inverter with novel PWM control scheme for PV application" IEEE Trans. Power Electronics, vol. 57, no. 6, pp. 2111-2123, Jun. 2010 | [8] C. T. Pan, W. C. Tu, and C. H. Chen, "A novel GZV-based multilevel single phase inverter" Taiwan Power Electronics conference, pp. 1391-1396, Sep. 2010. | [9]W. Yu, J. S. Lai, H. Qian, C. Hutchens, J. Zhang, G. Lisi, A. Djabbari, G. Smith, and T. Hegarty "High-efficiency inverter with H6-type configuration for photovoltaic non-isolated AC module applications" IEEE Applied power Electronics Conference and Exposition, pp. 1056- 1061, 2010. | [10] S. Vazquez, J. I. Leon, J. M. Carrasco, L. G. Franquelo, E. Galvan, M. Reyes, J. A. Sanchez, and E. Dominguez "Analysis of the power balance in the cells of a multilevel cascaded H- bridge converter" IEEE Trans. Industrial Electronics, vol. 57, no. 7, pp. 2287-2296, Jul. 2010. | [11] S. Daher, J. Schmid, and F. L.M. Antunes "Multilevel inverter topologies for stand-alone PV systems" IEEE Trans. Industrial Electronics, vol. 55, no. 7, pp. 2703-2712, Jul. 2008. | [12] M. Meinhardt and G. Cramer, "Past, present and future of grid connected photovoltaic and hybrid-power-systems" IEEE-PES Summer Meeting, pp. 1283-1288, 2000. | [13] S. Kouro, J. Rebolledo, and J. Rodriguez "Reduced switching frequency modulation algorithm for high-power multilevel inverters"IEEE Trans. Industrial Electronics, vol. 54, no. 5, pp. 2894-2901, Oct. 2007. | [14] W. Yu, C. Hutchens, J. S. Lai, J. Zhang, G. Lisi, A. Djabbari, G. Smith, and T. Hegarty, "High Efficiency Converter with Charge Pump and Coupled Inductor for Wide Input Photovoltaic AC Module Applications," IEEE Energy Conversion Congress and Exposition, pp. 3895-3900, 2009